A Cell Outage Management Framework for Dense Heterogeneous Networks

Oluwakayode Onireti, *Member, IEEE*, Ahmed Zoha, *Member, IEEE*, Jessica Moysen, *Student Member, IEEE*, Ali Imran, *Member, IEEE*, Lorenza Giupponi, *Senior Member, IEEE*, Muhammad Ali Imran, *Senior Member, IEEE*, and Adnan Abu-Dayya, *Senior Member, IEEE*

***Abstract*—In this paper, we present a novel cell outage management (COM) framework for heterogeneous networks with split control and data planes—a candidate architecture for meeting future capacity, quality-of-service, and energy efficiency demands. In such an architecture, the control and data functionalities are not necessarily handled by the same node. The control base stations (BSs) manage the transmission of control information and user equipment (UE) mobility, whereas the data BSs handle UE data. An implication of this split architecture is that an outage to a BS in one plane has to be compensated by other BSs in the same plane. Our COM framework addresses this challenge by incorporating two distinct cell outage detection (COD) algorithms to cope with the idiosyncrasies of both data and control planes. The COD algorithm for control cells leverages the relatively larger number of UEs in the control cell to gather large-scale minimization-of-drive-test report data and detects an outage by applying machine learning and anomaly detection techniques. To improve outage detection accuracy, we also investigate and compare the performance of two anomaly-detecting algorithms, i.e., k-nearest-neighbor- and local-outlier-factor-based anomaly detectors, within the control COD. On the other hand, for data cell COD, we propose a heuristic Grey-prediction-based approach, which can work with the small number of UE in the data cell, by exploiting the fact that the control BS manages UE-data BS connectivity and by receiving a periodic update of the received signal reference power statistic between the UEs and data BSs in its coverage. The detection accuracy of the heuristic data COD algorithm is further improved by exploiting the Fourier series of the residual error that is inherent to a Grey prediction model. Our COM framework integrates these two COD algorithms with a cell outage compensation (COC) algorithm that can be applied to both planes. Our COC solution utilizes an actor-critic-based reinforcement learning algorithm, which optimizes the capacity and coverage of the identified outage zone in a plane, by adjusting the antenna gain and transmission power of the surrounding BSs in that plane. The simulation results show that the proposed framework can detect both data and control cell outage and compensate for the detected outage in a reliable manner.**

***Index Terms*—Cell outage compensation (COC), cell outage detection (COD), cell outage management (COM), heterogeneous cellular network, self-healing, self-organizing network (SON).**

I. Introduction

RECENTLY, extensive research and standardization efforts have been channeled toward the definition of the paradigm of self-organizing networks (SONs), which aim at achieving a substantial reduction in capital and operational expenditures (CAPEX and OPEX) by reducing human involvement in network operational tasks, while optimizing network coverage, capacity, and quality of service [1], [2]. SONs aim to replace the manual operational processes that have been executed in legacy cellular networks since their conception, such as configuration, postdeployment optimization, and troubleshooting, with autonomous functions called SON functions, such as self-configuration, self-optimization, and self-healing [1]–[3]. The main task within the self-healing functionality is autonomous cell outage detection (COD) and its compensation. Traditionally, cell outages have been manually detected. In some cases, cell outage can be detected by the manual analysis of fault alarms at the operations and maintenance center (OMC), whereas other detections require site visits or drive testing. This is an expensive process. In addition, it may take hours or days for the cell outage to be detected, thus resulting in pronounced reduction in capacity and quality of service and coverage gap [4], [5]. Once detected, the outage is compensated in an ad hoc and manual fashion, making the whole process extremely inefficient and unreliable. With an increasing scale of networks, automatic detection and compensation of cell outage has become a necessity, and it has been included in recent Third-Generation Partnership Project (3GPP) releases [6]. Therefore, the SON paradigm aims to replace these manual tasks with an autonomous process that is referred to as cell outage management (COM) [7]–[12]. COM can be further subdivided into COD and cell outage compensation (COC). COD aims to autonomously detect outage cells, i.e., cells that are not properly operating due to possible failures, e.g., external failure such as power supply or network connectivity, or even misconfiguration [4]–[6], [13]. On the other hand, COC refers to the automatic mitigation of the degradation effect of the outage by appropriately adjusting suitable radio parameters,

Manuscript received October 6, 2014; revised February 13, 2015 and April 7, 2015; accepted April 20, 2015. Date of publication May 8, 2015; date of current version April 14, 2016. This work was supported by the National Priorities Research Program under Grant 5-1047-2437 from the Qatar National Research Fund (a member of The Qatar Foundation). The statements made herein are solely the responsibility of the authors. The review of this paper was coordinated by Prof. Y. Zhou.

O. Onireti and M. A. Imran are with the Institute for Communication Systems, University of Surrey, Surrey GU2 7XH, U.K. (e-mail: o.s.onireti@surrey.ac.uk; m.imran@surrey.ac.uk).

A. Zoha and A. Abu-Dayya are with the Qatar Mobility Innovations Center, P.O. Box 210531, Doha, Qatar (e-mail: ahmedz@qmic.com; adnan@qmic.com).

J. Moysen and L. Giupponi are with the Centre Tecnòlogic Telecomunicacions Catalunya, 08860 Barcelona, Spain (e-mail: lorenza.giupponi@cttc.es; jessica.moysen@cttc.es).

A. Imran is with the University of Oklahoma, Norman, OK 73019 USA (e-mail: ali.imran@ou.edu).

Color versions of one or more of the figures in this paper are available online at http://ieeexplore.ieee.org.

Digital Object Identifier 10.1109/TVT.2015.2431371

such as pilot power, antenna tilt, and azimuth of the surrounding cells. The degree of compensation is usually dictated by the operator's policies, which also specify the level of performance that must be satisfied in the outage region [9].

A few algorithms have already been proposed in the literature, e.g., in [4] and [13]–[18], as well as [8]–[11], for COD and COC, respectively. The COD problem has been addressed in [4] by leveraging the neighbor cell list NCL reports to construct a visibility graph, whose topology changes are used to detect cells that are experiencing outage. In [13], a weighted combination of three hypotheses, which was based on the distribution of the channel quality indicator (CQI), time correlation of the CQI differential, and registration request frequency, was used in detecting cell outage. Just recently, interest has emerged in applying methods from the machine learning domain, such as clustering algorithms [16] as well as Bayesian networks [18], to automate the detection of faulty cell behavior. Coluccia *et al.* [17] analyzed the variations in the traffic profiles for third-generation cellular systems to detect real-world traffic anomalies. In terms of COC, Amirijoo *et al.* in [8] and [9] investigated the effectiveness of control parameters, such as the reference signal power, antenna tilt, scheduling parameters, and the uplink target received power level, in mitigating the effect of cell outage. In [10], Li *et al.* proposed an autonomic particle swarm compensation algorithm with fast convergence speed, which is a key requirement in COC.

All these works have focused on the traditional homogeneous deployments, where only macrocells are deployed. However, future cellular deployments are expected to be heterogeneous and extremely dense. In this context, macrocells will provide the user equipment (UE) with ubiquitous experience, whereas dense small-cell deployments operating in bandwidths with heterogeneous characteristics will facilitate high-data-rate transmissions to a reduced number of UEs. At the same time, conventional heterogeneous deployments pose a number of challenges in terms of network management and energy consumption, as a result of the increased number of cells [19]. To mitigate these challenges, a new heterogeneous network (HetNet) architecture with split control and data planes has been recently proposed as a candidate for fifth-generation architecture [20]–[27]. In such an architecture, the control and data planes are separated and are not necessarily handled by the same node. Consequently, this gives the network operator more flexibility, since the small/data cells can be activated on demand to deliver UE-specific data only when and where needed, while the macro/control cells manage UE connectivity and mobility [24]. Thus, the separated plane architecture allows for improved mobility management performance, since the radio resource control (RRC) layers of the UEs and other control messaging, such as paging, will be handled by the control cells. In addition, the energy consumption is improved, since the proposed architecture also leads to longer data cell sleep periods, due to their on-demand activation. Note that, contrary to the newly proposed HetNet architecture, the RRC layers of all UEs in the conventional HetNet are handled by their serving cell, which could be either a small cell or a macrocell.

Only recently, Wang *et al.* [5] proposed a cooperative COD scheme for small cells in a conventional HetNet, whereas Xue *et al.* [28] proposed a COD scheme for detecting both macrocell and small-cell outages in a conventional HetNet. However, accurate small COD with [28] requires a fairly large number of UEs in each small cell, which, therefore, limits its usage. Furthermore, COC solutions for HetNets have been proposed in [29] and [30]. In [29], handover to macro is proposed as a solution for an outage caused by a small cell, whereas a collaborative resource allocation approach is proposed for UEs that cannot be served by the macrocell in [30]. Although individual COC and COD algorithms have been presented in the literature for conventional deployments, a complete COM framework, particularly for HetNets with split control and data planes, is still missing. The main difference in the COM framework in HetNets with split control and data planes and the conventional HetNet is in their architecture. In the traditional HetNet, control and data functionalities are provided to the UE by the same node, whereas these functionalities are provided by separate nodes in the split architecture. Hence, in the conventional architecture, an outage to a node can be compensated by any other node, whereas in the split architecture, an outage to a node can only be compensated by another node that provides the same functionalities. In this paper, we propose a complete COM framework, which is composed of concrete solutions for COD and COC, for a HetNet with separated control and data plane functionalities, and with different spectrum resources allocated to each plane.

Our framework has two distinct COD algorithms to cope with the peculiarities of data and control cells. Since control cells tend to have a large number of UEs, we exploit large-scale collection of minimization of drive test (MDT) reports, introduced by 3GPP in [31], and we apply machine-learning-based anomaly detection schemes for control COD. Thus, control COD can be implemented at the OMC level. In the control COD solution, we compare the performance of two anomaly-detecting algorithms, i.e., k-nearest neighbor anomaly detector (k-KNNAD) and local outlier factor anomaly detector (LOFAD), to find the best. However, the same COD scheme cannot be applied for data cells, as the number of users will not be large enough to constitute reliable training models for underlying anomaly detection techniques. Hence, we propose a heuristic data COD scheme, which works despite of the small number of UEs in the data cell, by exploiting a Grey prediction model (GM) for detecting data cell outage.

Once the outage is properly detected, we need to implement an online automatic COC scheme to continue serving the UEs in the outage area. Considering the acute dynamics of the always varying wireless environment in general and the high variability in terms of load fluctuations, in dense wireless deployments, we propose an actor critic (AC)-based reinforcement learning (RL) algorithm, which allows for learning online, through interactions with the surrounding environment, the best possible policy to compensate for the outage. The solution is based on optimizing the coverage and capacity of the identified outage zone, by adjusting the gains of the antennas through electrical tilt, and downlink transmission power of the surrounding base stations (BSs) in that plane. The proposed COC algorithm can be applied independently in each plane, as different spectrum resources are allocated to each plane.

The main contributions of this paper can be summarized as follows: 1) We propose a novel COM framework for the HetNet with split control and data planes; 2) we design, evaluate, and compare novel COD solutions for detecting control and data cell outages in the split architecture; and 3) we define an AC-RL algorithm, which can be used for both the control and data COC in the split architecture. The remainder of this paper is organized as follows. In Section II, we present the system architecture, which includes a description of the split architecture, the system model, and the COM framework. In Section III, we propose low-dimensional embedding of the MDT measurement for control COD. In Section IV, we introduce a heuristic-based data COD scheme. Section V presents an AC-based RL algorithm for both control and data COC. In Section VI, we present extensive simulations to substantiate the performance of our proposed COM framework for HetNets with separated control and data planes. Finally, Section VII concludes this paper.

II. System Architecture

A. Split Architecture

We consider the new paradigm of HetNet architecture, where the data and control/signaling planes are decoupled at the air interface, as recently proposed in [20]–[24]. The control plane provides ubiquitous network access and is made up of macro BSs, which we refer to as control BSs. On the other hand, the data plane supports high-data-rate transmission and is composed of the small BSs, which we call data BSs. The control plane handles UE connectivity as well as different radio-specific functions, which primarily cover 1) RRC connection management, 2) system information broadcast and synchronization, 3) configuration and measurement reporting, and 4) cell handover and network controlled mobility. In contrast, the data plane handles UE-specific data, and its functionalities are unicast and synchronization [23], [24]. Consequently, UEs requiring high-data-rate transmission are connected to both the control and data BSs, whereas low-rate UEs are connected to just the control BS.

B. System Model

We consider that the control and data BSs are operated on separate frequency carriers, so that there is no interference between the two planes. We assume that the HetNet is composed of a set of $\mathcal{M}$ macro BSs/control BSs and $\mathcal{F}$ small BSs/data BSs, where $M{=}|\mathcal{M}|$ control BSs form a regular hexagonal network layout with intersite distance D and provides coverage over the entire network. We denote the transmission power vector of control BS $m \in \mathcal{M}$ by $\mathbf{p}^m = (p_1^m, \ldots, p_R^m)$, where p_r^m is the downlink transmission power of resource blocks (RBs) r, and the maximum transmission power of each control BS, i.e., $P_{\max}^{\mathrm{m}}$, is such that $\sum_{r=1}^{R} p_r^m \leq P_{\max}^{\mathrm{m}}$. The $F{=}|\mathcal{F}|$ data BSs are randomly distributed. Similarly, we denote the transmission power vector of data BS $f{\in}\mathcal{F}$ by $\mathbf{p}^f = (p_1^f, \ldots, p_R^f)$, where p_r^f is the downlink transmission power of RB r, and the maximum transmission power of each data BS, i.e., $P_{\max}^{f}$, is such that $\sum_{r=1}^{R} p_r^f \leq P_{\max}^{\mathrm{f}}$. We also consider that U_m and U_f UEs are provided with service by the $\mathcal{M}$ control BSs and $\mathcal{F}$ data BSs, respectively. The multiuser resource assignment to the R RBs in a plane is carried out by a fractional frequency reuse (FFR) scheduler, and each of the UEs in the plane is assigned a CQI value. The FFR scheme, at the beginning of each subframe, divides each cell into two regions and assigns a certain group of RBs to the inner region and another, orthogonal, to the outer region, at the border of the cell. The inner regions of all the cells in the scenario are covered by the same spectrum (f), whereas the outer regions are assigned orthogonal RBs such as $\{f_1, \ldots, f_7\}$, as shown in Fig. 1 (FFR1). The latter also represents the amount of bandwidth reserved for the outage zone during COC (see FFR2 in Fig. 1).

C. COM Framework

In the HetNet architecture described earlier in Section II-B, outage can occur to a BS in either the control or the data plane, i.e., control or data BS outage, thus leading to a degradation in system performance. To alleviate the effect of such outage, the BS in outage has to be detected first. This can be achieved by monitoring deviations from the key performance indicator measurement report of the fault-free network. Thereafter, the parameters of BSs neighboring the outage BS in a given plane can be adjusted according to the operator's policy so as to compensate for the outage situation. Hence, we propose a COM framework, which primarily consists of the COD and COC stages.

1) COD: As mentioned earlier, active high-data-rate UEs are served by both the data and control BSs, whereas the low-rate UEs are served by only the control BS. This implies that all UEs maintain connectivity with the control BS. Furthermore, as a result of the split of the control and data planes, the control and data cell outages are independent of each other; hence, the detection of a cell outage in each plane is executed independently of the other. As shown in Fig. 1, our framework has two distinct COD algorithms to cope with the idiosyncrasies of the control and data cell. The control cell tends to have a large number of users; hence, large-scale data collection and machine learning is used for the control COD. Consequently, our control COD scheme is based on the MDT functionality, where all UEs report their MDT measurements, which include reference signal received power (RSRP) of the serving and neighboring cells, to the OMC vis respective BS. A normal network profile is built based on the measurements in a nonoutage scenario. The control COD is then performed at the OMC, by using anomaly detection algorithms, such as K-KNNAD and LOFAD, on the actual network profile.

However, this approach is not applicable for data COD, where UE statistics are sparse, due to the small number of UEs connected to each data BS. The control BS knows the location of every data BS in its coverage, and it can passively monitor the RSRP measurements of every UE-data BS association within its coverage. Consequently, a heuristic scheme, which can effectively leverage on the small number of reports and the fact that the control BS can monitor the UE-data BS association, is

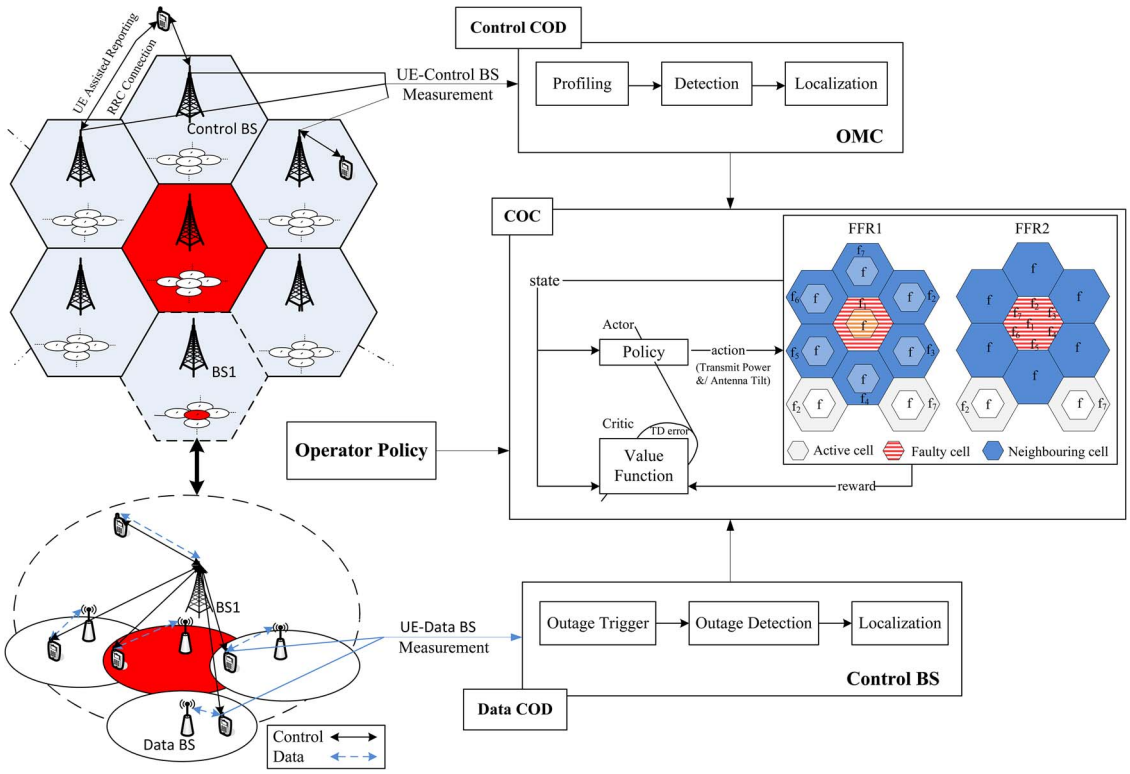

Fig. 1. Overview of the COM framework.

used for the data COD. The data COD is executed at the control BS and is triggered when the control BS detects irregularities in UE-data BS associations, whereas the actual detection is performed by using a GM algorithm.

2) COC: After the control or data cell outage has been detected by the OMC or by the control BS, respectively, an AC-RL COC scheme is implemented independently in both planes, as shown in Fig. 1. Note that no interplane interference is experienced since both planes are operated on separate carrier frequencies, and hence, the COC implementation in one plane has no impact on the other plane.

III. Control Cell Outage Detection via Low-Dimensional Embedding of Minimization of Drive Test Measurement

The main idea behind our control COD framework is to use the MDT reports acquired from a fault-free operating scenario to profile the behavior of the network. The goal is to use the learned profile to address the control cell outage autonomously. The proposed control COD framework adopts a four-step-based approach: 1) measurement, 2) profiling, 3) detection, and 4) localization. Each step is further elaborated in the following sections.

A. Measurement

The MDT reporting schemes have been defined in Long-Term Evolution (LTE) Release 10 [31], [32]. The release proposes constructing a database of MDT reports from the network using *Immediate* or *Logged* MDT reporting configuration. In this paper, the UEs are configured to report the cell identification and radio measurement data to the target control BS, based on the immediate MDT configuration procedure, as shown in Fig. 2. The signaling flow of the MDT reporting procedure consists of 1) configuration, 2) measurement, 3) reporting, and 4) storing phase. The UE is first configured to perform measurements periodically, as well as whenever an A2 event (i.e., serving cell becomes worst than a *threshold*) occurs. Subsequently, the UE performs measurements as specified in Table I and further reports them to the control BS. The control BS, after retrieving these measurements, further appends time and wideband CQI to these measurements and forwards them to the trace collection entity (TCE). The TCE collects and stores the trace reports, which are subsequently processed to construct

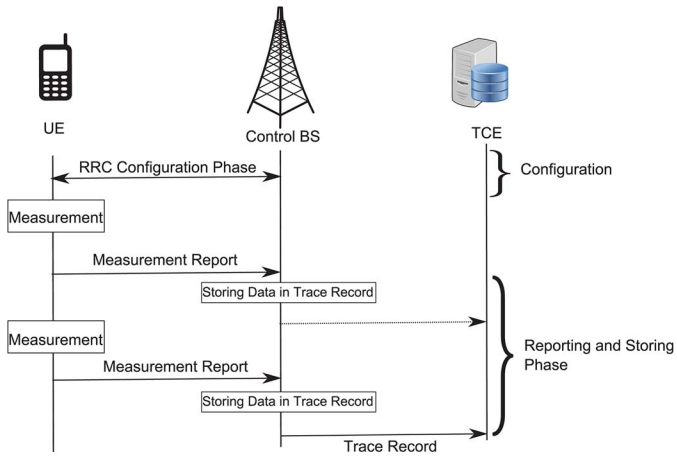

Fig. 2. Immediate MDT signaling flow.

TABLE I
MDT REPORTED MEASUREMENTS

Measurement	Description
Location	Longitude and latitude information
Serving cell information	E-UTRAN cell global identification (ECGI)
RSRP	Reference signal received power (RSRP) in dBm
RSRQ	Reference signal received quality (RSRQ) in dB
Neighboring cell information	Three strongest intra-LTE RSRP, RSRP information

an MDT database. The trace record obtained from the reference scenario (i.e., fault-free) acts as a benchmark data and is used by the anomaly detection models to learn the network profile. These models are then employed to autonomously detect outage situations.

B. Profiling

In the profiling phase, the trace records are processed to extract the feature vector $\mathbf{O}$ corresponding to each MDT measurement. The measurements including RSRP and quality of service as well as of the three strongest neighboring cells and the CQI are concatenated into a feature vector, i.e., $\mathbf{O}$, which is expressed as follows:

$$\mathbf{O} = [RSRP_S, RSRP_{n1}, RSRP_{n2}, RSRP_{n3}, RSRQ_S \quad RSRQ_{n1}, RSRQ_{n2}, RSRQ_{n3}, CQI] \quad (1)$$

where subscripts S and n denote the serving and neighboring cells, respectively. The observation vector, i.e., $\mathbf{O}$, is a 9-D vector of numerical features, which corresponds to one network measurement. To reduce the complexity of storage, processing, and analysis, this 9-D vector is embedded to three dimensions in the Euclidean space using the multidimensional scaling (MDS) method [33]. MDS provides low-dimensional embedding of the target measurement vectors $\mathbf{O}$ while preserving the pairwise distances among them. Given a $t \times t$ dissimilarity matrix $\boldsymbol{\Delta}^{\boldsymbol{X}}$ of the MDT data set, MDS attempts to find t data points $\psi_1, \ldots, \psi_t$ in m dimensions, such that $\boldsymbol{\Delta}^{\boldsymbol{\Psi}}$ is similar to $\boldsymbol{\Delta}^{\boldsymbol{X}}$. Classical MDS operates in Euclidean space and minimizes the following objective function:

$$\min_{\psi} \sum_{i=1}^{t} \sum_{j=1}^{t} \left(\phi_{ij}^{(X)} - \phi_{ij}^{(\Psi)} \right)^2 \quad (2)$$

where $\phi_{ij}^{(X)} = \|x_i - x_j\|^2$, and $\phi_{ij}^{(\Psi)} = \|\psi_i - \psi_j\|^2$. Equation (2) can be reduced to a simplified form by representing $\boldsymbol{\Delta}^{X}$ in terms of a kernel matrix using

$$\mathbf{X}^T\mathbf{X} = -\frac{1}{2}\mathbf{H}\boldsymbol{\Delta}^{\boldsymbol{X}}\mathbf{H} \quad (3)$$

where $\mathbf{H} = \mathbf{I} - \frac{1}{t}\mathbf{e}\mathbf{e}^T$, and $\mathbf{e}$ is a column vector of all 1's. Hence, (2) can be rewritten as

$$\min_{\psi} \sum_{i=1}^{t} \sum_{j=1}^{t} \left(x_i^T x_j - \psi_i^T \psi_j \right)^2. \quad (4)$$

As shown in [33], $\boldsymbol{\Psi}$ can be obtained by solving $\boldsymbol{\Psi} = \sqrt{\boldsymbol{\Lambda}}\mathbf{V}^T$, where $\mathbf{V}$ and $\boldsymbol{\Lambda}$ are the matrices of top m eigenvectors and the corresponding eigenvalues of $\mathbf{X}^T\mathbf{X}$, respectively. The m-dimensional embedding of the data points is the rows of $\sqrt{\boldsymbol{\Lambda}}\mathbf{V}^T$, whereas the value of m is chosen to be 3 in our case. The preprocessing of the network observation $\mathbf{O}^e$ using the MDS method has several advantages. In the literature, the MDS technique has been widely used as a dimensionality reduction method [33]–[35] to transform high-dimensional data into a meaningful representation of reduced dimensionality. One of the problems with high-dimensional data sets is that, in many cases, not all of the measured variables are "critical" for understanding the underlying phenomena. As shown in the literature, dimensionality reduction is a critical preprocessing step for the analysis of real-world data sets, since it mitigates the curse of dimensionality and other undesired properties of high-dimensional space [36]. MDS aims to achieve an optimal spatial configuration in low-dimensional space, such that distances in the new configuration (i.e., $\phi_{ij}^{(\Psi)}$) are close in value to the observed distances (i.e., $\phi_{ij}^{(X)}$). The spatial configurations help reveal a hidden structure that is not obvious from raw data matrices, allowing to explore the interrelationships of high-dimensional space. Given the growing complexity of the networks, particularly in the case of a SON, it is challenging to identify few measurements that accurately capture the behavior of the system. The MDS preprocessing of the network measurements allows to achieve a reduced representation that corresponds to intrinsic dimensionality of data. Consequently, the low-dimensional representation of network measurements facilitates data modeling and allows the anomaly detection algorithms to obtain better estimation of data density. As a result, the anomalous network measurements can be detected with higher accuracy, as discussed below. Moreover, unlike other dimensionality reduction methods such as principal component analysis or linear discriminant analysis, MDS does not make an assumption of linear relationships between the variables and, hence, is applicable to a wide variety of data.

In addition to network measurements, each MDT report is tagged with the location and time information, as listed in Table I, which is used in conjunction with RSRP values to estimate the dominance or the coverage area of each target control BS in the network. The dominance map estimation is further used to autonomously localize the position of the outage control BS.

The next step after preprocessing is to develop a reference database, i.e., $\mathbf{D}_M$, by storing the embedded measurements that represent the normal operation of the network. As shown in Fig. 3, this reference database is used by a state-of-the-art anomaly detection algorithm to learn the "normal" network profile. The goal of this algorithm is to define an anomaly detection rule that can differentiate between normal and abnormal MDT measurements by computing a threshold "φ" based on

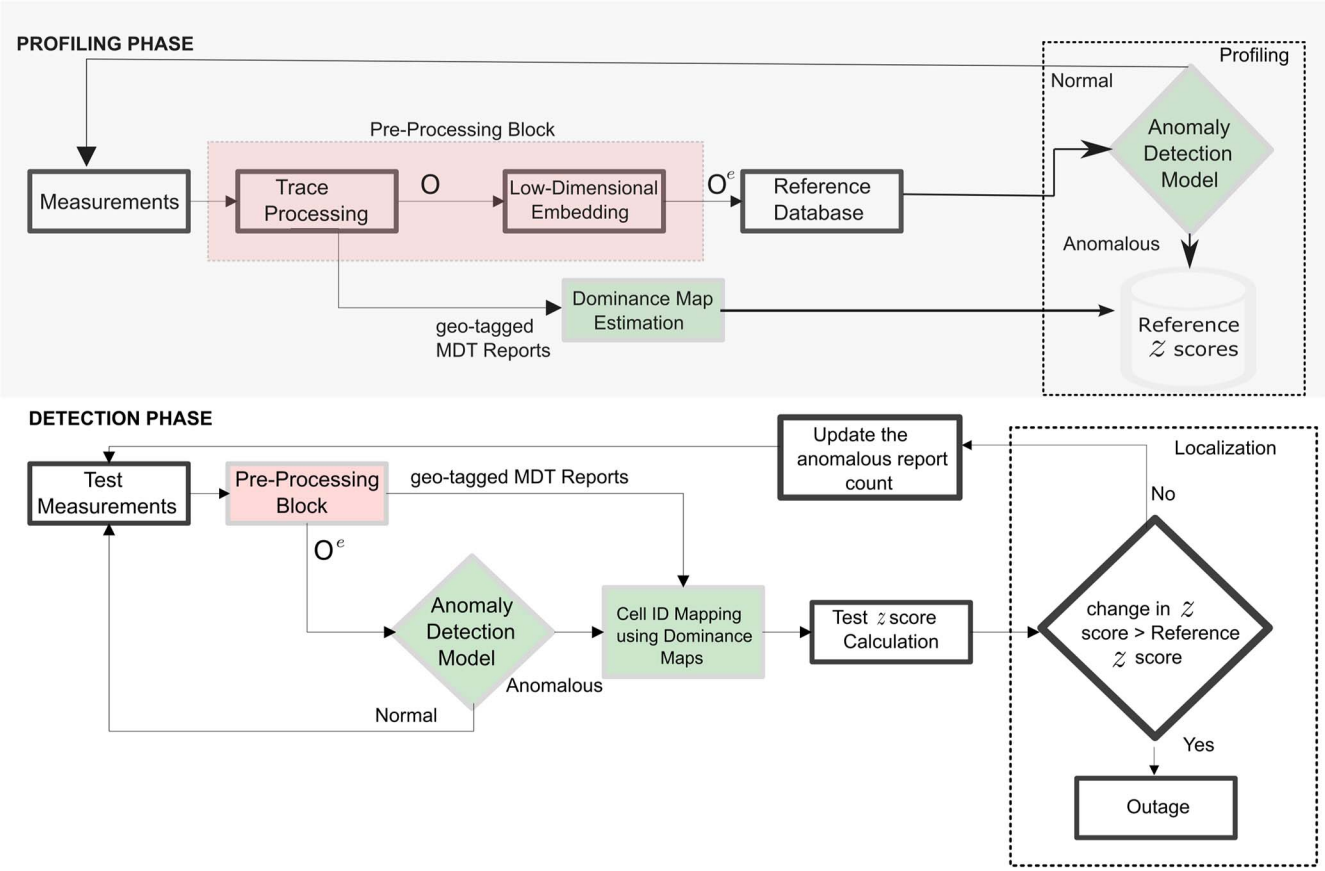

Fig. 3. Overview of profiling and detection phases in the control COD framework.

a dissimilarity measure $\mathcal{D}$. Thus, it can be treated as a binary classification problem, which can formally be expressed as follows:

$$f(x_i) = \begin{cases} \text{Normal}, & \text{if } \mathcal{D}(x_i, \mathbf{D}_M) \leq \varphi \\ \text{Anomalous}, & \text{if } \mathcal{D}(x_i, \mathbf{D}_M) > \varphi. \end{cases} \tag{5}$$

Two state-of-the-art anomaly detection algorithms, namely, k-KNNAD and LOFAD, are examined in our study. Anomalies, depending on their position in the MDS space, can be categorized as *local* or *global*. Local anomalies are localized to a small spatial region (i.e., local density) or a neighborhood, whereas global anomalies are bounded to the entire data set (i.e., global densities). k-NNAD computes a global dissimilarity measure $\mathcal{D}_{k-\text{NNAD}}$, which assigns a score to the test observation x_i based on its distance from the kth nearest training point in the MDS space. On the other hand, LOFAD, instead of the distance measure, compares the local density of x_i to its k neighbors and correspondingly assigns a score. The correct profiling of the network behavior is dependent on the accuracy of the anomaly detection models. The two anomaly detection algorithms are briefly summarized as follows.

1) k-KNNAD: Let x_i be the test instance and k be the kth neighbor in the $\mathbf{D}_M$. To label x_i as normal or abnormal, k-KNNAD computes $\mathcal{D}_{k-\text{NNAD}}$ as

$$\mathcal{D}_{k-\text{NNAD}}(x_i, k, \mathbf{D}_M) = \frac{1}{N_{tr}} \sum_{i=1}^{N_{tr}} \mathcal{I}(d_t \leq d_i) \tag{6}$$

where $N_{tr} = |\mathbf{D}_M|$, d_t is the distance of x_i from its kth nearest neighbor, d_i is the distance between i and its kth nearest training object in $\mathbf{D}_M$, and $\mathcal{I}(.)$ is an indicator function. The indicator function is activated as soon as the condition $d_t \leq d_i$ is fulfilled. The expression in (6) represents a global density-based anomaly detection score, as proposed in [37]. The test measurement is marked anomalous if it receives a score greater than the φ value.

2) LOFAD: The LOFAD [38] tries to compare the local density, i.e., ρ, of the object to that of its k neighbors. It constructs a local neighborhood of an instance x_i and defines its distance to the kth nearest neighbor $NN(x_i, k)$, i.e.,

$$d_b(x_i, k) = d\left(x_i, NN(x_i, k)\right). \tag{7}$$

$d_b(x_i, k)$ is used to construct a neighborhood $\mathcal{N}(x_i, k)$ by including all those points, which fulfills the criteria: $d(x_i, x_j) \leq d_b(x_i, k)$. Formally, reachability distance d_r is defined to estimate $\rho(x_i, k)$ as follows:

$$d_r(x_i, k) = \max\left\{d_b(x_j, k), d(x_j, x_i)\right\} \tag{8}$$

and ρ can be defined as

$$\rho(x_i, k) = \frac{|\mathcal{N}(x_i, k)|}{\sum_{x_j \in \mathcal{N}(x_i, k)} d_r(x_i, x_j, k)}. \tag{9}$$

$d_r(x_i, x_j, k)$ ensures that instances that lie farther away from x_i have less impact on $\rho(x_i, k)$. Finally, $\mathcal{D}$ can be calculated

by comparing the ρ of x_i to its $\mathcal{N}(x_i, k)$, which is formally defined as

$$\mathcal{D}_{\text{LOFAD}}(x_i, k; \mathbf{D}_{\text{train}}) = \frac{\sum_{x_j \in \mathcal{N}(x_i,k)} \frac{\rho(x_j,k)}{\rho(x_i,k)}}{|\mathcal{N}(x_i, k)|}. \quad (10)$$

$\mathcal{D}_{\text{LOFAD}}$ represents a local density-estimation score; a value close to 1 means x_i has the same density as its neighbors. On the other hand, a significantly high $\mathcal{D}_{\text{LOFAD}}$ score is an indication of anomaly.

The parameter selection for k-NNAD and LOFAD is performed using a cross-validation (CV) method, as described in Algorithm 1.

Algorithm 1 Model Selection Using CV Method

1: Split the target data set $\mathbf{D}_M$ into K chunks.
2: **for** $l = 1, 2, \ldots, K$: **do**
3: Set $\mathbf{D}_{val}$ to be the lth chunk of data.
4: Set $\mathbf{D}_{\text{train}}$ to be the other $K - 1$ chunks.
5: Fit each model of $\mathbf{D}_{\text{train}}$ and evaluate its performance on $\mathbf{D}_{val}$.
6: **end for**
7: **Model Selection:** Select the model with an average highest detection score.

The $\mathbf{D}_M$ is divided into training $\mathbf{D}_{\text{train}}$ and validation data set $\mathbf{D}_{val}$ using K-fold approach, where the value of K is chosen to be 10 in our framework. To select the optimal model, each target detector is trained for different values of k, and the model achieving the average highest detection score is selected.

As shown in Fig. 3, the control COD during the profiling phase calculates the reference z-score for each target control BS in the network using the benchmark data. The z-score is calculated as follows: $z_b = (|N_b - \mu_n|/\sigma_n)$, where N_b is the number of MDT reports labeled as anomalies by the anomaly detection model for the target control BS b, and variables μ_n and σ_n are the mean and standard deviation anomaly scores of the neighboring cells. In the profiling phase, we also estimate the so-called dominance area, i.e., for each cell, we define the area where its signal is strongest. To do this, we exploit the location information tagged with each measurement report, which will then allow us to associate a cell and the corresponding z-scores, as shown in Fig. 3. The calculation of the dominance area along with the corresponding reference z-score for each control BS in the network would allow us to detect an outage control cell situation autonomously in the detection phase, as discussed in the following section.

C. Detection and Localization Phase

In the detection phase, the test measurements are preprocessed in a similar fashion as in the profiling phase. The embedded representation $\mathbf{V}^e$ is classified as normal or anomalous by the anomaly detection models. Subsequently, the geolocation of each report is correlated with the estimated dominance maps (i.e., profiled during the profiling phase) to establish its correct cell association. This is because as soon as the control cell outage situation is triggered in the network, the malfunctioning control BS becomes no longer available. Consequently, the dominance or the coverage area of the neighboring cells increases, to serve the affected area. Therefore, if only E-UTRAN cell global identification (ECGI) information is utilized to localize the outage control cell, the anomalous MDT reports within the target area would erroneously be associated to its neighboring cells. The label assigned by the anomaly detection model to each measurement in conjunction with its estimated cell ID is used to calculate the test z-score in the outage scenario. Finally, the control cell outage situation is detected and localized by observing the change in the z-score obtained for each control BS in the outage scenario compared with the reference scenario.

IV. Data Cell Outage Detection via Heuristic Approach

Contrary to the control COD, which is performed at the OMC, the data COD is performed at each control BS. Hence, establishing the normal state of the control BS is a prerequisite for data COD. The data COD process is organized into the trigger and detection phases, as shown in Fig. 4. All UEs associated with the data BS report their RSPP statistics to their serving control BS, which is later used in the detection process.

A. Outage Trigger Phase

The control BS receives a periodic update of the RSRP of the link between each UE and its associated data BS and stores this value in a database. As mentioned earlier in Section II-A, the control BS is responsible for managing UE connectivity and radio-specific functions, such as 1) RRC connection, 2) configuration and measurement reporting, and 3) cell handover and network controlled mobility. Consequently, the control BS is aware of any change in UE-data BS association, as a result of handover or radio link failure. The control BS is also aware of any state change in the UE, such as a change from active to idle state, from idle to detached state, and *vice versa*. Furthermore, the conditions for the data BS to enter sleep mode are known to the control BS. For example, the data BS could be allowed to enter the sleep mode if the number of active UEs is lower than a certain predefined threshold during the last scheduling time interval.

In the outage trigger phase, the control BS monitors the UE-data BS association and triggers the outage detection when it discovers irregularities in UE-data BS association. Irregularities in UE-data BS association occur when all UEs attached to a particular data BS change their association with none of the following: 1) prior handover initiation process, 2) change in state of all the UEs, 3) radio link failure notification from all the UEs, 4) the data BS going into sleep mode.

B. Outage Detection Phase

Once the outage detection phase is triggered, the control BS can detect outage of the data BS by predicting the RSRP of all the UEs that were associated with it prior to the outage. We utilize the GM, which has been extensively used in handover, positioning, and general forecasting algorithms [39]–[43], as a prediction model.

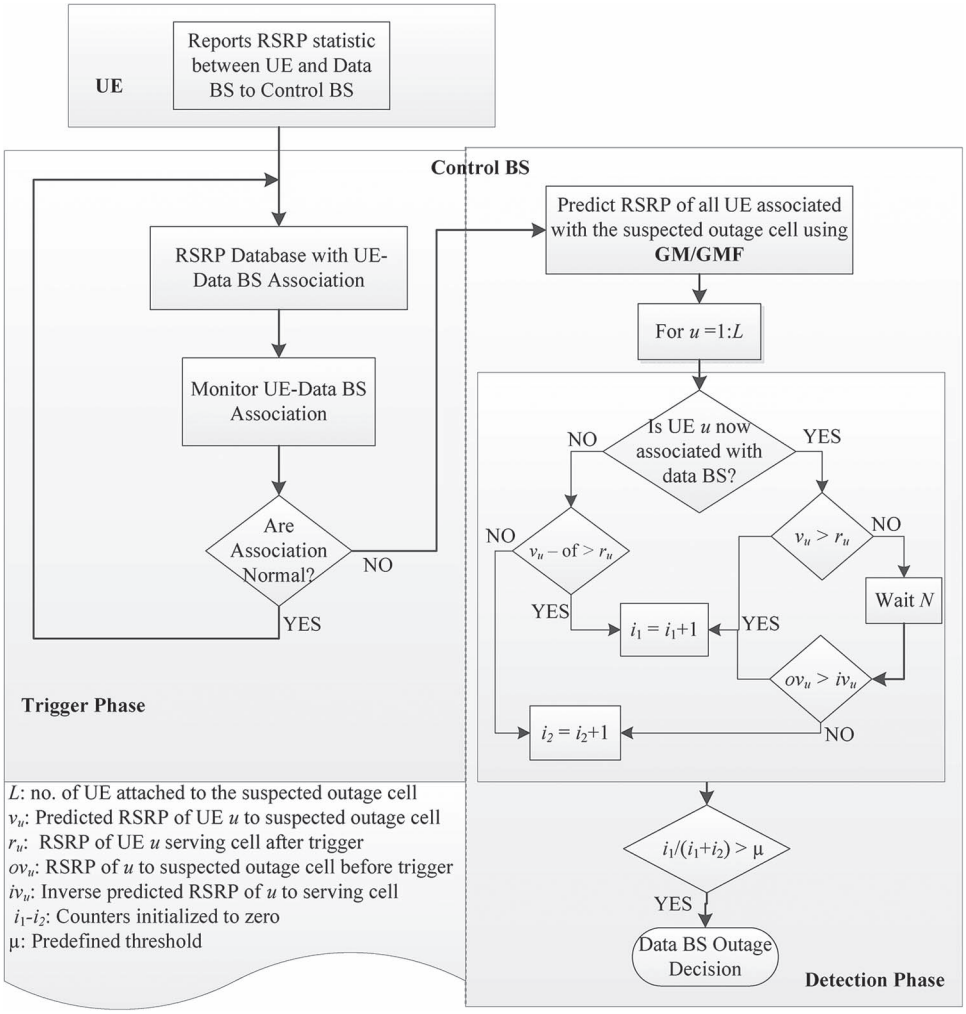

Fig. 4. Data COD flowchart.

1) GM Approach: In Grey system theory, $GM(\bar{n}, \bar{m})$ denotes a Grey model, where $\bar{n}$ is the order of the differential equation, and $\bar{m}$ is the number of variables. Here, we focus on $GM(1,1)$, which is a widely used time-series forecasting model. According to [39], the $GM(1,1)$ model can only be used on positive data sequences. Note that the RSRP values are always positive; hence, the Grey model can be used to predict the next RSRP value from data points obtained in the database.

The three basic operations in Grey prediction are 1) the accumulated generating operation (AGO), 2) the inverse accumulated generating operation (IAGO), and 3) Grey modeling. By using AGO, an irregular raw data can be transformed into a regular data, which can be used to construct a model in a Grey differential equation. The nonnegative RSRP data sequence of UE u prior to the outage is denoted as

$$r_u^{(0)} = \left(r_u^{(0)}(1), r_u^{(0)}(2), r_u^{(0)}(3), \ldots, r_u^{(0)}(n)\right) \quad \forall\, n \geq 4. \tag{11}$$

When the sequence given in (11) is subject to AGO, the following sequence, i.e., $r_u^{(1)}$, is obtained as

$$r_u^{(1)} = \left(r_u^{(1)}(1), r_u^{(1)}(2), r_u^{(1)}(3), \ldots, r_u^{(1)}(n)\right) \quad \forall\, n \geq 4 \tag{12}$$

where

$$r_u^{(1)}(c) = \sum_{i=1}^{c} r_u^{(0)}(i), \quad c = 1, 2, 3, \ldots, n \tag{13}$$

which results in the Grey differential equation given as

$$\frac{dr_u^{(1)}(t)}{dt} + a r_u^{(1)}(t) = b. \tag{14}$$

The coefficients, i.e., a and b, can be obtained by using the least squares method, as shown in

$$[a, b]^T = (B^T B)^{-1} B^T Y \tag{15}$$

where

$$Y = \left[r_u^0(2), r_u^0(3), \ldots, r_u^0(n)\right]$$
$$B = \begin{bmatrix} -h^1(2) & 1 \\ -h^1(3) & 1 \\ . & . \\ . & . \\ -h^1(n) & 1 \end{bmatrix} \tag{16}$$

and $h^{(1)}(c) = \alpha r_u^{(1)}(c) + (1-\alpha) r_u^{(1)}(c-1), c = 2, 3, \ldots, n$, α is the weighting factor.

Once a and b in (14) are obtained, the Grey differential equation can be used to predict the value of r_u at time instant $c+1$. The solution of $r_u^{(1)}(t)$ at time $c+1$, i.e., the AGO Grey prediction model, is expressed as

$$\hat{r}_u^{(1)}(c+1) = \left[r_u^{(0)}(1) - \frac{b}{a} \right] e^{-ac} + \frac{b}{a}, \quad c = 0, 1, \ldots. \tag{17}$$

Consequently, the prediction value of the benchmark RSRP data at time $(c+1)$ can be calculated by an IAGO as

$$\hat{r}_u^{(0)}(c+1) = \left[r_u^{(0)}(1) - \frac{b}{a} \right] e^{-ac}(1 - e^{a}). \tag{18}$$

2) GM Modification Using Fourier Series of Residual Error (GMF): According to [42], Grey model prediction accuracy can be improved by the Fourier series of error residuals. Consider the uth UE RSRP sequence $r_u^{(0)}$ in (11) and its predicted values obtained from (18), then the error of the sequence $r_u^{(0)}$ can be expressed as

$$\xi_u^{(0)} = \left(\xi_u^{(0)}(2), \xi_u^{(0)}(3), \ldots, \xi_u^{(0)}(n) \right) \tag{19}$$

where

$$\xi_u^{(0)}(c) = r_u^{(0)}(c) - \hat{r}_u^{(0)}(c), \forall\, c = 2, 3, \ldots, n. \tag{20}$$

The error residuals given in (20) can be reexpressed in Fourier series in the following approximation:

$$\xi_u^{(0)}(c) \approx \frac{1}{2} a_0 + \sum_{i=1}^{J} \left[a_i \cos\left(\frac{2\pi i}{T} c \right) + b_i \sin\left(\frac{2\pi i}{T} c \right) \right] \tag{21}$$

$\forall\, c = 2, 3, \ldots, n$, where $T = n-1$, and $J = \lfloor (n-1)/2 \rfloor - 1$. Note that the expression in (21) can further be reexpressed as

$$\xi_u^{(0)} \approx Q\mathcal{C} \tag{22}$$

where Q is given in (23), shown at the bottom of the page. Hence, $\mathcal{C}$ can be obtained by using the least squares method to solve (22) as

$$\mathcal{C} = (Q^T Q)^{-1} Q^T \xi_u^{(0)}. \tag{24}$$

The Fourier series correction is thus given according to [42] as

$$\hat{\hat{r}}_u^{(0)}(c) = \hat{r}_u^{(0)}(c) - \hat{\xi}_u^{(0)}(c) \quad \forall\, c = 2, 3, \ldots, n+1. \tag{25}$$

C. Outage Decision

Consider that the outage of data BS d, which has L UEs attached prior to the outage trigger, is to be detected. First, we define counters i_1 and i_2 and initialize their values to zero. The RSRP of the L UEs that were previously attached to the data BS, i.e., d, are predicted according to (18) or (25). Then, for each UE, the control BS compares its predicted RSRP value, i.e., $v_u = \hat{r}_u^{(0)}(c+1) \approx \hat{\hat{r}}_u^{(0)}(c+1)$, with the RSRP after the trigger, i.e., $r_u = r_u^{(0)}(c+1)$. If, afterward, outage is triggered, the UE, i.e., u, is served by the control BS for data transmission, and $v_u = \hat{r}_u^{(0)}(c+1) \approx \hat{\hat{r}}_u^{(0)}(c+1) > r_u - \Delta$, where Δ is the data cell range expansion offset, the counter, i.e., i_1, is incremented by 1, since the UE should be associated with the data BS, i.e., d, based on the prediction. Otherwise, the counter, i.e., i_2, is incremented by 1. On the other hand, if another data BS is serving UE u, after the outage trigger and $v_u \approx \hat{r}_u^{(0)}(c+1) \approx \hat{\hat{r}}_u^{(0)}(c+1) > r_u$, the counter, i.e., i_1, is incremented by 1; otherwise, an inverse prediction is performed on the RSRP to the serving data BS. The inverse prediction checks the RSRP to the data BS d and the RSRP to the serving data BS after the trigger, i.e., data BS $\bar{d}$, at the point just before the trigger. The control BS waits for the prediction window size, i.e., N, and performs an inverse prediction on the RSRP of each of the UEs associated with data BS $\bar{d}$ to obtain the predicted RSRP prior to the trigger decision, i.e., iv_u. Thus, if the RSRP of the uth UE to the serving data BS (d) before trigger, i.e., ov_u, is such that $ov_u > iv_u$, the counter i_1 is incremented by 1; otherwise, the counter i_2 is incremented by 1. The data cell outage is declared if the ratio $i_1/(i_1+i_2) > \mu$, where μ is a system predefined threshold.

V. Reinforcement Learning-Based Cell Outage Compensation

Here, we provide a complete solution for COC. We consider that the network has the capability to detect both data and control outages, through the solutions proposed in previous sections. We provide a solution capable of recovering both data and control outages. In particular, we consider an outage of a control BS in the control plane or a data BS in the data plane. Hence, we optimize the coverage and capacity at the identified outage zone, by adjusting the gain of the antenna through the electrical tilt and the downlink transmission power of the surrounding control/data BS in the control/data plane. To implement this approach, we propose an RL scheme, which has the capability of making online decisions at each control/data BS and of adapting to the evolution of the scenario, determined

$$Q = \begin{bmatrix} 0.5 & \cos\left(2\frac{2\pi}{T}\right) & \sin\left(2\frac{2\pi}{T}\right) & \cos\left(2\frac{2\pi 2}{T}\right) & \sin\left(2\frac{2\pi 2}{T}\right) & \ldots & \cos\left(2\frac{2\pi V}{T}\right) & \sin\left(2\frac{2\pi V}{T}\right) \\ 0.5 & \cos\left(3\frac{2\pi}{T}\right) & \sin\left(3\frac{2\pi}{T}\right) & \cos\left(3\frac{2\pi 2}{T}\right) & \sin\left(3\frac{2\pi 2}{T}\right) & \ldots & \cos\left(3\frac{2\pi V}{T}\right) & \sin\left(3\frac{2\pi V}{T}\right) \\ \ldots & \ldots & \ldots & \ldots & \ldots & \ldots & \ldots & \ldots \\ 0.5 & \cos\left(n\frac{2\pi}{T}\right) & \sin\left(n\frac{2\pi}{T}\right) & \cos\left(n\frac{2\pi 2}{T}\right) & \sin\left(n\frac{2\pi 2}{T}\right) & \ldots & \cos\left(n\frac{2\pi V}{T}\right) & \sin\left(n\frac{2\pi V}{T}\right) \end{bmatrix}$$

$$\text{and} \quad \mathcal{C} = \begin{bmatrix} a_0 & a_1 & b_1 & a_2 & b_2 & \ldots & a_n & b_n \end{bmatrix}^T \tag{23}$$

by factors such as the UE mobility, shadowing, and decisions made by the surrounding control/data BSs to the problem being solved.

A. RL

The RL aims to learn from interactions to achieve a certain goal. The learner or the decision maker is called *agent*, and it continuously interacts with the so-called *environment*. The agent selects actions, and the environment responds to those actions and evolves into new situations. In particular, the environment responds to the actions through *rewards*, numerical values, which the agent tries to maximize over time. The agent has to exploit what it already knows to obtain a reward, but it also has to explore to take better actions in the future. We assume that the environment is the wireless cellular scenario, with all its realistic characteristics, in terms of UE mobility and activity patterns, and channel variations, whereas the agents are the control/data BSs.

Let $\mathcal{S}$ be the set of possible states of the environment $\mathcal{S} = \{s_1, s_2, \ldots, s_n\}$ and $\mathcal{A}$ be a set of possible actions $\mathcal{A} = \{a_1, a_2, \ldots, a_q\}$ that each agent may choose. The interactions between the multiagent system and the environment at each time instant t consist of the following sequence.

- Control/data BS i senses the state $s_t^i = s \in \mathcal{S}$.
- Based on s, control/data BS i selects an action $a_t^i = a \in \mathcal{A}$.
- As a result, the environment makes a transition to the new state $s_{t+1}^i = v \in S$.
- The transition to state v generates a reward $r_t^i = r \in \Re$.
- The reward r is fed back to the control/data BS, and the process is repeated.

In the following, we remove the notation indicating the specific agent i, for the sake of simplicity. At each time step, the agent implements a mapping from states to probabilities of selecting each possible action. This mapping is the agent's *policy*. The objective of each learning process is to find an optimal policy $\pi^*(s) \in \mathcal{A}$ for each s to maximize some cumulative measure of reward r received over time. Almost all RL algorithms are based on estimating the so-called *value function*, which is a function of the states estimating how good it is for an agent to be in a given state. The quantification of this is defined based on the expected future rewards. Of course, the rewards that an agent can expect to receive in the future depend on what actions it will take. As a result, the value of a state s under a policy π, which is denoted $\mathcal{V}^\pi(s)$, is the expected return when starting in s and following π thereafter:

$$\mathcal{V}^\pi(s) = \mathbb{E}\left\{\sum_{t=0}^{\infty} \gamma^t r\left(s_t, \pi(s)\right) | s_t = s\right\} \tag{26}$$

where $\mathbb{E}$ stands for the expectation operator, and $0 \leq \gamma < 1$ is a discount factor. Considering the extreme complexity of the dynamics of the complete wireless cellular environments, where the UEs move around the scenario according to random mobility models, the channel is affected by path loss, fading, and shadowing, and the activity of UEs is again determined by random processes, we are not able to rely on a model of the environment's dynamic to solve this maximization problem. A solution is then to take advantage of the theory of RL and, in particular, of the so-called temporal difference (TD) learning approaches. These kinds of methods are able to learn directly from experience, without a model of the environment's dynamics. Among the literature of TD learning schemes, we select the AC approach to adjust the downlink transmission power levels of the control/data BSs surrounding the outage zone, as it is one of the most representative TD schemes, and it is not computationally complex. TD learning schemes can be proven to converge to optimal solutions, in stationary scenarios with only one decision maker, although in practice, they have been shown to provide successful results also in multiagent scenarios [44]. The proof of convergence of the learning algorithm is guaranteed by the Bellman optimality criterion [45]. Our solution is proposed for a multiagent system, where each agent self-adapts based on an AC algorithm, and the performances of each control/data BS are affected by the actions of the others in terms of intercell interference.

B. AC

The AC method is a TD method that has a separate memory structure to represent the policy independently of the value function. The policy structure is known as the *actor*, since it is used to select the actions, whereas the estimated value function is known as the *critic*. The critic learns and critiques whatever policy is currently being followed by the actor and takes the form of a TD error δ, which is used to determine if a_t was a good action or not. δ is a scalar signal, which is the output of the critic and drives the learning procedure. After each action selection, the critic evaluates the new state to determine whether things have gone better or worse than expected, as it is defined by the TD error, i.e.,

$$\delta_t = r_t + \gamma \mathcal{V}_t(s_{t+1}) - \mathcal{V}_t(s_t) \tag{27}$$

where $\mathcal{V}$ is the current value function implemented by the critic, to evaluate the action a_t taken in s_t. If the TD error is positive, it suggests that the tendency to select a_t should be strengthened for the future, whereas if the TD error is negative, it suggests that the tendency should be weakened. We identify this tendency with a preference function $P(s_t, a_t)$, which indicates the tendency or preference to select a certain action in a certain state. Then, the strengthening or weakening previously described can be implemented by increasing or decreasing $P(s_t, a_t)$ by

$$P(s_t, a_t) \leftarrow P(s_t, a_t) + \beta\, \delta_t \tag{28}$$

where β is a positive learning parameter. This is the simplest implementation of an AC algorithm. The variation that we consider for implementation is to add different weights to different actions, for example, based on the probability of selecting action a_t in state s_t, i.e., $\pi(s_t, a_t)$, which results in the following update rule:

$$P(s_t, a_t) \leftarrow P(s_t, a_t) + \beta\, \delta_t \left(1 - \pi(s_t, a_t)\right). \tag{29}$$

In this implementation, AC directly implements the Boltzmann exploration method to select actions as follows:

$$\pi(s_t, a_t) = \frac{e^{P(s_t,a_t)}}{\sum_{a_t \in \mathcal{A}} e^{P(s_t,a_t)/\tau}}. \quad (30)$$

This means that the probability to select an action a in state s at time t depends on the temperature parameter τ and on the preference values $P(s_t, a_t)$ at time t. In this kind of exploration, actions that seem more promising, because of higher preference values, have a higher probability of being selected.

1) AC-RL for COC: To design the AC algorithm to implement the automatic transmission power and antenna tilt adjustment for the COC, while mitigating the generated interference and improving the capacity of the zone, we need to define the state and action spaces and the reward function.

- *State*: The state is defined based on the result of the scheduling scheme, which defines 1) the allocation of UEs to RBs (i.e., $RB_1, RB_2, \ldots, RB_R$ to the N UEs in the plane) and 2) the values of the CQI of each UE in the corresponding RB.
- *Actions*: The sets of eligible actions are as follows.
  - The finite set of downlink transmission power levels, which can be allocated to the RBs assigned to the UEs. The selected values are 0–23 dBm per RB for the data BS and 0–46 dBm per RB for the control BS, each with 0.5-dBm granularity.
  - The finite set of available tilt values, which can be assigned to the gain of the vertical plane of the antenna model. Those values range from 0 to 15° with 0.5° granularity.
- *Reward*: The reward function is defined based on the signal-to-interference-plus-noise ratio (SINR) of the UEs as follows:

$$r(s_t, a_t) = \begin{cases} 1, & \text{if SINR} \geq -6 \\ 0, & \text{otherwise} \end{cases}$$

where the threshold is set to support the lowest modulation and coding scheme [9] for LTE.

To mitigate the intercell interference that the adjustment of the neighboring control/data BS power level may generate in the outage zone, frequency bandwidth $\mathcal{B} = \{f_1, \ldots, f_7\}$ is reserved for the UEs moving in the outage zone, while f serves UEs in each of neighboring cells to the outage BS, as shown in Fig. 1 (FFR2).

The learning algorithm is executed every 1 ms, which is also the smallest scheduling time interval in LTE. Hence, the solution of the learning algorithm can be applied when allocating UEs every time scheduling is performed. The execution of the learning algorithm at TTI resolution increases the speed with which the fault and the outage are recovered. However, it is possible to execute the algorithm less often, to reduce the computational complexity, but this will increase the time the system suffers from the outage generated by the fault. In practice, the operator implementing the algorithm can set the frequency of execution to the preferred value based on trading off the implementation criteria considered more important. We recommend that the learning algorithm must be executed with low periodicity during the emergency situation to speed up the recovery when many users have seen their quality of experience compromised and with higher periodicity when the outage is about to be fully recovered. The CQI is obtained from the spectral efficiency (η) provided in [46]. A high-level vision of the COC algorithm is shown in Fig. 1.

TABLE II
SIMULATION PARAMETERS

Parameter	Value
Tx Power Control BS	46 dBm
Tx Power Data BS	23 dBm
Path loss model	Friis spectrum propagation
Mobility model	pedestrian, speed 3 kmph, 60 kmph
UE distribution	Uniform random distribution
Scheduler	FFR
Shadow Fading	Log-normal, std = 2-10dB
AMC model	4-QAM, 16-QAM, 64 QAM
Macro cell layout	radius:500 m
Bandwidth per plane	5 MHz
No. of RBs	25; RBs per RBG:2
Antenna gain (Normal Scenario)	18 dBi
Antenna gain (Outage Scenario)	-50 dBi
MDT reporting interval	240 ms
Minimal sensible signal strength	-107.5 dBm
Detection threshold μ	0.5
Detection window size N	10
Grey weighting factor α	0.5
SINR threshold	-6 dB
Actions (Control BS power)	$0-46$ dBm per RB: Granularity 0.5 dBm
Actions (Data BS power)	$0-23$ dBm per RB: Granularity 0.5 dBm
Actions (tilt)	$0°-15°$: Granularity $0.5°$
Parameters τ, β, γ	0.1, 0.5, 0.98
Simulation time	10 minutes

VI. SIMULATION RESULTS AND DISCUSSIONS

A. Simulation Scenario

Here, we demonstrate the performance of our HetNet COM framework by presenting simulation results for the COD and COC algorithms. We consider a HetNet architecture where the control and data BSs operate on separate frequency carriers. Each operation mode occupies 5 MHz of channel bandwidth. The scenario that we set up consists of 27 macro/control BSs with $U_m = 20$ UEs per control BS and $FB = 5$ femtocell blocks per control BS, each one with $l = 40$ apartments, $t = 1$ floor, $d = 0.2$ small/data BS deployment ratio as per [47], and $c = 0.5$ data BS activation ratio, which results in 20 data BSs per control BS. Moreover, there are U_f UEs per data BS in the scenario. The principle of UE association is such that each UE associates with a control BS for signaling transmission. Furthermore, each UE associates with a data BS for data transmission if its RSRP from the data BS exceeds that of the control BS; otherwise, it associates with a control BS for both data and control signaling transmission. The parameters used in the simulations, for the cellular scenario, control and data COD algorithms, and the COC algorithm, are given in Table II.

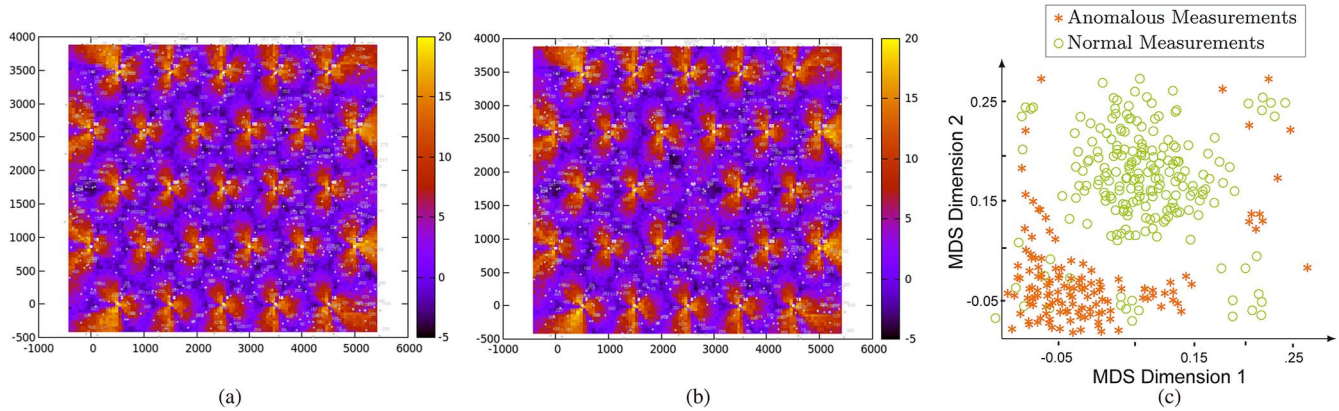

Fig. 5. (a) SINR plot of the reference scenario. (b) SINR plot of the control cell outage scenario, where the antenna gain of cell 11 is attenuated to −50 dBi. (c) MDT measurements in the embedded space classified into normal and anomalous categories by k-NNAD.

B. COD

We simulate the reference scenario to profile the normal network operation, in which all UEs are configured to report the MDT measurements on the control plane. In addition, UEs that are associated with the data cells are also configured to periodically report their RSRP statistics (in the data plane) to their serving control BS. A control cell outage scenario is simulated by attenuating the antenna gain of control BS 11 in the network to −50 dBi for a duration of 3 min. The total simulation run time was 10 min for each scenario. Likewise, for the data cell outage, we focus of on control BS 10 and attenuate the antenna gain of data BS 11 within its coverage to −50 dBi. The respective SINR plots of the reference and outage scenario in the control plane is shown in Fig. 5. The collected measurements are processed by our proposed control and data COD frameworks, as shown in Figs. 3 and 4, respectively.

1) Control COD: Local and global anomaly detection approaches, namely, LOFAD and k-NNAD, have been compared to select the final model for profiling the network behavior. The receiver operating characteristic (ROC) curves [48] plot the true positive rate or the detection rate (DR; i.e., a percentage of anomalous measurements correctly classified as anomalies) against the false positive rate (FPR; i.e., a percentage of normal cell measurements classified as anomalies). The ROC curves are generated by plotting the DR against the FPR by varying φ for each model until a DR value reaches 100%. To access the performance of the target algorithms, a standard performance metric named area under ROC (AUC) curve is employed. To select the optimal model for each anomaly detector, a parameter search (i.e., $k = 1, 2, \ldots, 30$) is performed using Algorithm 1. The final values of k are found to be 20 and 8 for k-NNAD and LOFAD, respectively.

It has been observed that measurements that conform to the normal behavior of network operations, when projected to embedded space, group themselves into a large cluster. On the other hand, when the measurements belonging to the outage control cell scenario are projected to the embedded space, they lie far from the dense cluster of normal measurements, as shown in Fig. 5(c). The reason is that MDS embedding of the measurements maximizes the variance between the data points, and consequently, dissimilar points are projected far from each other. This embedded representation of measurements reveals a hidden structure of data. In particular, this is helpful for the density-based anomaly detection models as employed in this study, to learn an effective anomaly detection rule. Since such models assume that anomalous data lie in low-density regions, the embedded representation of the data aids in establishing a boundary between high- and low-density regions. Consequently, an effective anomaly detection rule can be learned. The k-NNAD-based global profiling technique, which relies on the global density estimation procedures, outperforms local density estimation method LOFAD, since the anomalous measurements obtained from the outage scenario largely act as global anomalies. Moreover, some of the normal measurements also form small microclusters. This is due to exceptionally good RSRP values reported by the mobile terminals while they are in close proximity to the serving control BS. However, LOFAD treats them as local anomalies. Additionally, the measurements obtained from the cell edges show similarity with data samples that correspond to the outage scenario. Hence, in the embedded space, they are projected close to the samples that correspond to abnormal measurements. From a classification perspective, the target models wrongly classify such measurements as belonging to an outage control cell scenario. However, from a SON perspective, identification of such abnormality indicates a weak coverage problem and can be used to trigger automated actions for coverage optimization. Similarly, some of the UE-generated measurements, as a result of radio link failure, are also treated as anomalies. Fig. 6 shows that k-NNAD achieves 80% DR, which is 15% higher than LOFAD at a false alarm rate of 10%. As shown in Table III, the AUC values achieved by k-NNAD and LOFAD are 0.91 and 0.85, respectively, which shows the superiority of global anomaly detection methods over local approaches for profiling the network behavior.

We use k-NNAD as our target model to calculate the z-score for each control BS, separately, for reference and control cell outage scenarios, as shown in Fig. 7. It can be observed that even the cells that are not in outage receive a z-score, since a fraction of the UE reported measurements, belonging to their dominance areas, are identified as anomalies for the reasons discussed earlier. Therefore, to classify a cell as in outage, each control BS must collect a minimum number of

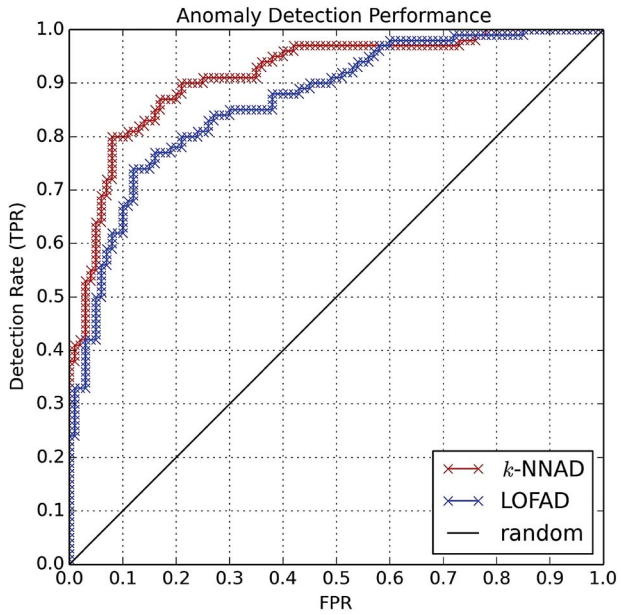

Fig. 6. ROC curve of the k-NNAD-based profiling technique.

TABLE III
PERFORMANCE OF TARGET ANOMALY DETECTION MODELS FOR CONTROL COD

[t] Model	Approach	AUC score
k-NNAD	Global	0.91
LOFAD	Local	0.85

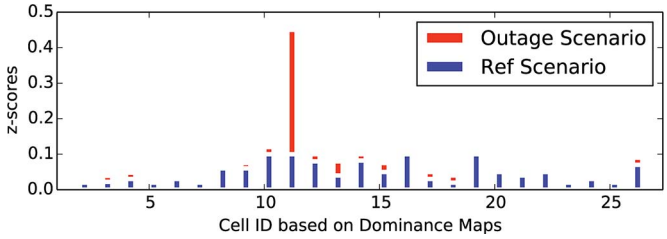

Fig. 7. Cell dominance areas versus z-scores for localization of control cell outage.

anomalous reports (i.e., N_b) to achieve a significantly higher z-score compared with the rest of cells. We collect approximately 4800 measurements in 1 min from each cell, since our scenario is characterized by 20 uniformly distributed UEs that send reports with a periodicity of 240 ms.

The z-scores shown in Fig. 7 for each control cell are normalized by the total number of measurements obtained every minute. It can be observed that the outage cell (i.e., control cell 11) achieves the highest percentage z-score of 0.449 ($N_b = 3520$, with mean and standard deviation values of neighboring cells as 500 and 140, respectively), which is above our heuristically set threshold of 0.3. The test z-score of the outage cell significantly deviates from its reference z-score of 0.09, and it can be easily detected. Likewise, the delay value can increase or decrease, depending on the UE density in the target cell.

2) Data COD: Fig. 8 shows the performance of our data COD framework in terms of the DR. In Fig. 8(a), we compare the performance of the GM and GMF, which are obtained from (18) and (25), respectively, with the cooperative COD approach in [5], by plotting their DR against the data cell UE density, i.e., U_f, and for shadowing fading standard deviation of $\sigma = 2$ and 10 dB. For the cooperative COD scheme, we consider the cooperative range as the coverage area of each control BS. We observe that the proposed schemes, which are also independent of the cooperative range, outperform the cooperative COD scheme in [5]. We observe that the GMF scheme outperforms the GM as expected, since the former utilizes the prediction error in the latter to improve its performance. Fig. 8(a) clearly shows that increasing the UE density increases the DR. This is due to the fact that increasing UE density enables a better spatial correlation. Fig. 8(b) shows the DR for various data BS power levels and a data cell UE density of $U_f = 3(/100\text{ m} \times 100\text{ m})$. The result shows that low data BS transmission power results in degradation of the DR, whereas increasing the transmission power leads to an improvement in the DR. This is because when the data BS transmission power increases, it becomes easier to distinguish between the predicted RSRP statistics of the outage case and the normal case. We also observe in Fig. 8(a) and (b) that the DR becomes lower with larger shadowing fading standard deviation σ. This is because a high σ means severe shadowing fading, which leads to a more random RSRP statistics.

Fig. 9(a) and (b) investigates the impact of the predefined threshold μ and prediction window size $\mathcal{N}$, respectively, on the DR. We observe in Fig. 9(a) that the highest DR is obtained by setting $\mu = 0.5$. This setting implies that the RSRP prediction of more than half of the UEs that were associated with the data BS whose outage is being detected, i.e., d, must indicate the existence of an outage, before d can be declared to be in outage. The stepwise shaped plot is obtained since the number of UEs must be an integer value. We also observe that there is not much degradation in DR until $\mu > 0.67$, which implies that more than two thirds of UEs that were associated with d must indicate the existence of an outage. In Fig. 9(b), we observe that increasing the prediction window size above the required minimal ($\mathcal{N} = 4$) leads to an increase in DR up to a point where any further increase in $\mathcal{N}$ has no impact on the DR. Fig. 9(b) further shows that increasing $\mathcal{N}$ has more impact on the DR for larger shadow fading standard deviation, i.e., σ. This is because of the lower randomness in RSRP statistics when σ is low; hence, a low value of $\mathcal{N}$ is required to obtain the highest attainable DR, which is the contrary for higher σ, where a higher value of $\mathcal{N}$ is required.

C. COC

Here, we consider that outage occurs when data BS 11 in control BS 10 fails to provide service to its associated UEs. We assume that the data COD framework in the previous section has already detected the problem, and we therefore focus on the COC solution. Here, the neighboring cells are in charge of adjusting their power transmission and antenna tilt to fill the coverage gap. We start by analyzing the behavior of a UE

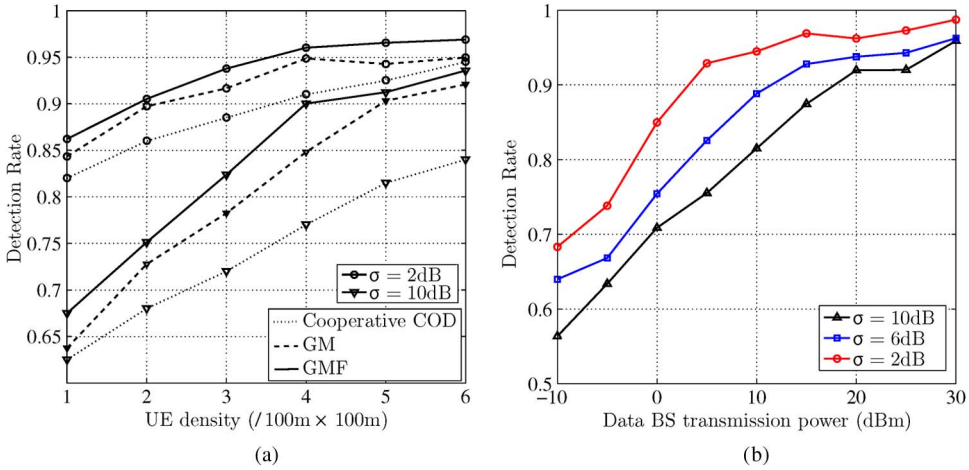

Fig. 8. Performance of the data COD framework. (a) GM versus GMF. (b) Effect of data BS transmission power on DR.

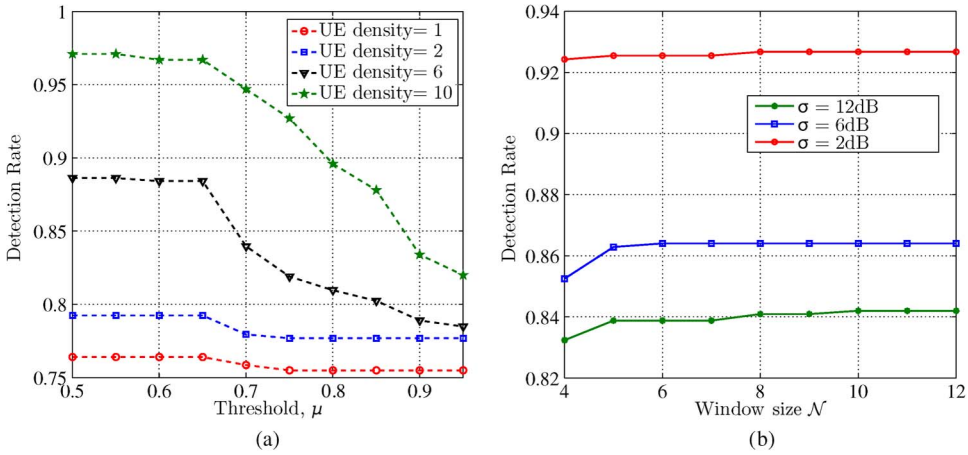

Fig. 9. Effect of data COD algorithm parameters on DR. (a) Effect of threshold setting on DR. (b) Effect of window size on DR.

attached to the faulty data BS. We observe that once the COC algorithm is operational, the UE gets associated to one of the neighboring data BSs, which we refer to as the *compensating cell*. The CQI associated to the UE in this moment is zero. The scheduling scheme is implemented to minimize the interference generated from compensating cells, by reserving a certain RB group (RBG) to the UE. This information is shared with neighbor data BSs through the X2 interface. We refer to the AC algorithm in Section V, where both the Tx power and antenna tilt are adjusted, as the AC(p + θ).

Fig. 10 shows the time evolution of the SINR of the UE from the instant the data cell outage is detected and the COC algorithm starts working until it is recovered and correctly associated to the compensating cell. We show the behavior of the algorithm for both pedestrian (3 km/h) and vehicular (60 km/h) scenarios. We observe that in both cases, the COC algorithm takes advantage of its capability of making online decisions, properly adapting to the evolution of the environment, even when it is varying quickly, as it happens in vehicular settings. We assume that the UE is recovered when its SINR is above the threshold, which is set to -6 dB, as explained in Section V-B1. The behavior followed by the AC(p + θ) scheme is such that, during the first part of the simulation, it learns the proper policy to recover the UE from outage through interactions with the environment. After approximately 450–500 ms, for the pedestrian and vehicular cases, respectively, the UE SINR

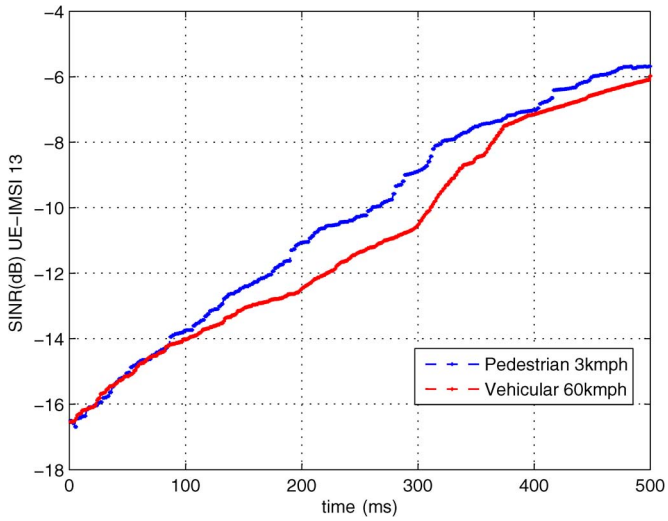

Fig. 10. Time evolution of the average SINR of UE 13, which is recovered from outage by the COC solution based on AC.

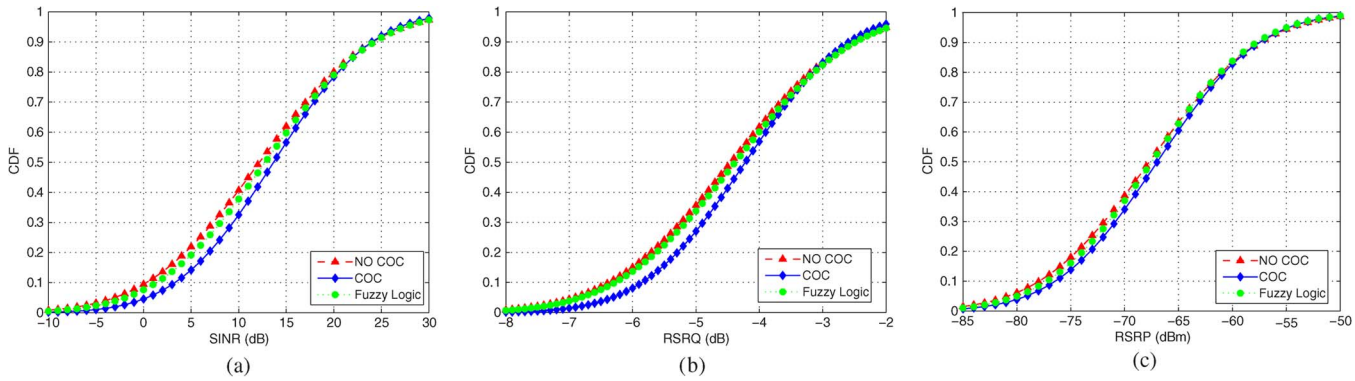

Fig. 11. Comparison of the cdf of the SINR, RSRQ, and RSRP of the COC with fuzzy logic and NO COC. (a) CDF of the SINR of the serving cells. (b) CDF of the RSRQ of the serving cells. (c) CDF of the RSRP of the serving cells.

reaches the threshold and maintains higher values during the rest of the simulation. Since the correct policy has been learnt, it can be maintained independently of the variations in the scenario, such as UE mobility, random data BS activity factor, etc. Fig. 10 further shows that the performance in high mobility (vehicular) is worse compared with the pedestrian case; hence, a slightly longer time is required to recover from outage in the high mobility.

Fig. 11 shows the performances of our COC framework in terms of SINR, RSRQ, and RSRP of the UEs, which are represented by means of the cumulative distribution function (cdf), and compared with the case where no COC scheme is implemented, i.e., NO COC in the figures, and to the state-of-the-art benchmark, discussed in [49] and based on fuzzy logic theory. Fig. 11(a) represents the cdf of the SINR of the UEs in the scenario, after convergence of the learning approach. It shows that the proposed AC$(\mathrm{p}+\theta)$ scheme performs better than both the NO COC option and the fuzzy logic scheme. Fig. 11(b) shows the cdf of the RSRQ of the UEs in the scenario, after convergence of the learning approach. Here, again, we observe that the AC$(\mathrm{p}+\theta)$ scheme provides better results than the fuzzy logic approach and the NO COC scheme. Finally, Fig. 11(c) shows that the proposed AC$(\mathrm{p}+\theta)$ scheme provides better results also in terms of RSRP than the fuzzy logic and the NO COC schemes.

D. COM Framework Cost

Here, we give some insight on the cost associated with implementing the proposed COM framework. The cost metric encompasses the complexity in analysis, processing, storage, and signaling overhead. A large part of the cost associated with our proposed COM framework lies in the control COD, as it requires a large number of users and measurement reports to achieve a high DR. This cost has been substantially reduced in our control COD solution by employing an MDS method, which embeds each network measurement from a 9-D feature vector into three dimensions in Euclidean space. Furthermore, the data COD solution in our framework is implemented in a fully distributed fashion at each control BS, thus significantly reducing the implementation cost of the framework. COC solutions, on the other hand, are implemented in a semidistributed fashion by dividing the system into clusters, where each cluster contains the outage cell and its neighbors, thereby reducing the signaling overhead and processing cost of the framework.

VII. Conclusion

In this paper, we have presented a novel COM framework for HetNets with split control and data planes. Two distinct COD algorithms have been proposed, taking into account an expected large number of UEs in the control cells and a small number of UEs in the data cells. For control COD, we have utilized the large-scale data gathering of MDT reports, as recently standardized by 3GPP in Release 10. The solution exploits MDS techniques to reduce the complexity of data processing while retaining pertinent information to develop training models to reliably apply anomaly detection techniques. Furthermore, within the control COD, we have compared the performance of two anomaly-detecting algorithms, i.e., k-NNAD and LOFAD. We found out that k-NNAD, which is a global anomaly detection model, achieved higher detection accuracy of up to 94% compared with LOFAD, which adopts a local approach for classifying abnormal measurement. On the other hand, for data cell outage, we have utilized a heuristic Grey prediction approach, which can reliably work despite of the small number of UEs in the data cells by exploiting the information stemming from the fact that the control BS manages the UE connectivity to the data BS within its coverage. The simulation results have shown that both control and data COD schemes can detect control and data cell outages, respectively, in a reliable manner. In addition, we have proposed an AC-based RL algorithm, which can be applied for both the control and data COC. The proposed COC algorithm solution was based on optimizing the coverage and capacity of the identified outage zone, by adjusting the gains of the antennas through electrical tilt and downlink transmission power of the surrounding BSs in that plane. Simulation results have shown that the AC-RL algorithm can recover all UEs from outage within a very short time.

Acknowledgment

The authors would like to thank the members of the University of Surrey 5G Innovation Center for their support.

REFERENCES

[1] J. L. Van den Berg *et al.*, "Self-organisation in future mobile communication networks," in *Proc. ICT Mobile Summit*, Stockholm, Sweden, pp. 1–9, 2008.

[2] O. G. Aliu, A. Imran, M. A. Imran, and B. G. Evans, "A survey of self organisation in future cellular networks," *IEEE Commun. Surveys Tuts.*, vol. 15, no. 1, pp. 336–361, 1st Quart. 2013.

[3] R. Combes, Z. Altman, and E. Altman, "Self-organization in wireless networks: A flow-level perspective," in *Proc. IEEE INFOCOM*, Mar. 2012, pp. 2946–2950.

[4] C. Mueller, M. Kaschub, C. Blankenhorn, and S. Wanke, "A cell outage detection algorithm using neighbor cell list reports," in *Proc. Int. Workshop Self-Organizing Syst.*, 2008, pp. 218–229.

[5] W. Wang, J. Zhang, and Q. Zhang, "Cooperative cell outage detection in self-organizing femtocell networks," in *Proc. IEEE INFOCOM*, Apr. 2013, pp. 782–790.

[6] *3rd Generation Partnership Project; Technical Specification Group Services and System Aspects; Telecommunications Management; Self-Organizing Networks (SON); Self-Healing Concepts and Requirements (Release 11)*, 3GPP TS 32.541, 2012-09, v11.0.0, 2012.

[7] M. Amirijoo *et al.*, "Cell outage management in LTE networks," in *Proc. ISWCS*, Sep. 2009, pp. 600–604.

[8] M. Amirijoo, L. Jorguseski, R. Litjens, and L.-C. Schmelz, "Cell outage compensation in LTE networks: Algorithms and performance assessment," in *Proc. IEEE VTC Spring*, 2011, pp. 1–5.

[9] M. Amirijoo, L. Jorguseski, R. Litjens, and R. Nascimento, "Effectiveness of cell outage compensation in LTE networks," in *Proc. IEEE CCNC*, 2011, pp. 642–647.

[10] W. Li, P. Yu, Z. Jiang, and Z. Li, "Centralized management mechanism for cell outage compensation in LTE networks," *Int. J. Distrib. Sensor Netw.*, vol. 2012, 2012, Art. ID. 170 589.

[11] L. Fuqiang, Q. Xuesong, W. Honglin, T. Zhengxian, and M. Luoming, "An algorithm of cell outage compensation in wireless access networks," *Int. J. Advance. Comput. Technol.*, vol. 4, no. 1, pp. 404–414, Jan. 2012.

[12] A. Zoha, A. Saeed, A. Imran, M. A. Imran, and A. Abu-Dayya, "A SON solution for sleeping cell detection using low-dimensional embedding of MDT measurements," in *Proc. IEEE PIMRC*, Washington, DC, USA, pp. 1–5, Sep. 2014.

[13] Q. Liao, M. Wiczanowski, and S. Stanczak, "Toward cell outage detection with composite hypothesis testing," in *Proc. IEEE ICC*, Jun. 2012, pp. 4883–4887.

[14] R. Barco, V. Wille, and L. Díez, "System for automated diagnosis in cellular networks based on performance indicators," *Eur. Trans. Telecommun.*, vol. 16, no. 5, pp. 399–409, Sep./Oct. 2005.

[15] B. Cheung, S. G. Fishkin, G. N. Kumar, and S. A. Rao, "Method of monitoring wireless network performance," U.S. Patent 10/946 255, Sep. 21, 2004.

[16] Y. Ma, M. Peng, W. Xue, and X. Ji, "A dynamic affinity propagation clustering algorithm for cell outage detection in self-healing networks," in *Proc. IEEE WCNC*, Apr. 2013, pp. 2266–2270.

[17] A. Coluccia, A. D'Alconzo, and F. Ricciato, "Distribution-based anomaly detection via generalized likelihood ratio test: A general maximum entropy approach," *Comput. Netw.*, vol. 57, no. 17, pp. 3446–3462, Dec. 2013.

[18] R. Khanafer *et al.*, "Automated diagnosis for UMTS networks using Bayesian network approach," *IEEE Trans. Veh. Technol.*, vol. 57, no. 4, pp. 2451–2461, Jul. 2008.

[19] D. Lopez-Perez *et al.*, "Enhanced intercell interference coordination challenges in heterogeneous networks," *IEEE Wireless Commun. Mag.*, vol. 18, no. 3, pp. 22–30, Jun. 2011.

[20] S. Liu, J. Wu, C. H. Koh, and V. K. N. Lau, "A 25 Gb/s(/km^2) urban wireless network beyond IMT-advanced," *IEEE Commun. Mag.*, vol. 49, no. 2, pp. 122–129, Feb. 2011.

[21] A. Capone, I. Filippini, B. Gloss, and U. Barth, "Rethinking cellular system architecture for breaking current energy efficiency limits," in *Proc. SustainIT ICT*, 2012, pp. 1–5.

[22] H. Ishii, Y. Kishiyama, and H. Takahashi, "A novel architecture for LTE-B: C-plane/U-plane split and phantom cell concept," in *Proc. GC Wkshps*, Dec. 2012, pp. 624–630.

[23] X. Xu, G. He, S. Zhang, Y. Chen, and S. Xu, "On functionality separation for green mobile networks: Concept study over LTE," *IEEE Commun. Mag.*, vol. 51, no. 5, pp. 82–90, May 2013.

[24] A. Zakrzewska, D. López-Pérez, S. Kucera, and H. Claussen, "Dual connectivity in LTE HetNets with split control- and user-plane," in *Proc. IEEE GC Wkshps*, Dec. 2013, pp. 391–396.

[25] A. Mohamed *et al.*, "Physical layer frame in signalling-data separation architecture: Overhead and performance evaluation," in *Proc. Eur. Wireless Conf.*, May 2014, pp. 1–6.

[26] A. Mohamed, O. Onireti, M. A. Imran, and R. Tafazolli, "Correlation-based adaptive pilot pattern in control/data separation architecture," in *Proc. IEEE ICC*, London, U.K., pp. 1–6, 2015.

[27] T. Alsedairy, Y. Qi, A. Imran, M. A. Imran, and B. Evans, "Self organizing cloud cells: A resource efficient network densification strategy," *Trans. Emerging Telecommun. Technol.*, 2014, to be published.

[28] W. Xue, M. Peng, Y. Ma, and H. Zhang, "Classification-based approach for cell outage detection in self-healing heterogeneous networks," in *Proc. IEEE WCNC*, Apr. 2014, pp. 2822–2826.

[29] W. Xue, H. Zhang, Y. Li, D. Liang, and M. Peng, "Cell outage detection and compensation in two-tier heterogeneous networks," *Int. J. Antennas Propag.*, vol. 2014, 2014, Art. ID. 624 858.

[30] K. Lee, H. Lee, and D.-H. Cho, "Collaborative resource allocation for self-healing in self-organizing networks," in *Proc. IEEE ICC*, 2011, pp. 1–5.

[31] *Universal Mobile Telecommunications System (UMTS); LTE; Universal Terrestrial Radio Access (UTRA) and Evolved Universal Terrestrial Radio Access (E-UTRA); Radio Measurement Collection for Minimization of Drive Tests (MDT); Overall Description; Stage 2*, 3GPP TS 37.320, 2011-04, v10.1.0 Release 10, 2011.

[32] S. Hämälïnen, H. Sanneck, and C. Sartori, *LTE Self-Organising Networks (SON): Network Management Automation for Operational Efficiency*. Hoboken, NJ, USA: Wiley, 2012.

[33] T. Cox and M. A. Cox, *Multidimesional Scaling*. Boca Raton, FL, USA: CRC, 2010.

[34] P. Pawliczek and W. Dzwinel, "Interactive data mining by using multidimensional scaling," *Procedia Comput. Sci.*, vol. 18, pp. 40–49, 2013.

[35] H. Bunke, P. Dickinson, A. Humm, C. Irniger, and M. Kraetzl, "Computer network monitoring and normal event detection using graph matching and multidimensional scaling," in *Advances in Data Mining. Applications in Medicine, Web Mining, Marketing, Image and Signal Mining*, Berlin, Germany: Springer-Verlag, 2006, pp. 576–590.

[36] R. Kharal, "Semidefinite embedding for the dimensionality reduction of DNA microarray data," M.S. thesis, Dept. Comput. Sci., Univ. Waterloo, Waterloo, ON, Canada, 2006.

[37] M. Zhao and V. Saligrama, "Outlier detection via localized p-value estimation," in *Proc. Annu. Allerton Conf. Commun., Control, Comput.*, 2009, pp. 1482–1489.

[38] M. M. Breunig, H.-P. Kriegel, R. T. Ng, and J. Sander, "LOF: Identifying density-based local outliers," in *Proc. SIGMOD Conf.*, 2000, pp. 93–104.

[39] B. L. Deng, "Introduction to Grey system," *J. Grey Syst.*, vol. 1, no. 1, pp. 1–24, 1989.

[40] S.-T. Sheu and C.-C. Wu, "Using Grey prediction theory to reduce handoff overhead in cellular communication systems," in *Proc. IEEE PIMRC*, 2000, vol. 2, pp. 782–786.

[41] C.-H. Lee and C.-J. Yu, "An intelligent handoff algorithm for wireless communication systems using Grey prediction and fuzzy decision system," in *Proc. IEEE ICNSC*, 2004, pp. 541–546.

[42] E. Kayacan, B. Ulutas, and O. Kaynak, "Grey system theory-based models in time series prediction," *Expert Syst. Appl.*, vol. 37, no. 2, pp. 1784–1789, Mar. 2010.

[43] R. Luo, O. Chen, and S. Pan, "Mobile user localization in wireless sensor network using Grey prediction method," in *Proc. 31st Annu. Conf. IEEE Ind. Electron. Soc.*, 2005, pp. 2680–2685.

[44] L. Panait and S. Luke, "Cooperative multi-agent learning: The state of the art," *Auton. Agents Multi-Agent Syst.*, vol. 3, pp. 383–434, Nov. 2005.

[45] R. S. Sutton and A. G. Barto, *Reinforcement Learning: An Introduction*. Cambridge, MA, USA: MIT Press, 1998.

[46] P. Giuseppe, N. Baldo, and M. Miozzo, "An LTE module for the ns-3 network simulator," in *Proc. SimuTOOLS*, Barcelona, Spain 2011, pp. 415–422.

[47] *Simulation Assumptions and Parameters for FDD HeNB RF Requirements*, 3GPP R4-092042, 2009.

[48] A. P. Bradley, "The use of the area under the ROC curve in the evaluation of machine learning algorithms," *Pattern Recognit.*, vol. 30, no. 7, pp. 1145–1159, Jul. 1997.

[49] A. Saeed, O. Aliu, and M. Imran, "Controlling self healing cellular networks using fuzzy logic," in *Proc. IEEE WCNC*, Paris, France, Apr. 2012, pp. 3080–3084.

Oluwakayode Onireti (S'11–M'13) received the B.Eng. degree (first-class grade) in electrical engineering from the University of Ilorin, Ilorin, Nigeria, in 2005 and the M.Sc. degree (with distinction) in mobile and satellite communications and the Ph.D. degree in electronics engineering from the University of Surrey, Surrey, U.K., in 2009 and 2012, respectively.

He is currently a Research Fellow with the Institute for Communication Systems, University of Surrey. He has been actively involved in European-Commission-funded projects such as ROCKET and EARTH. His main research interests include self-organizing cellular networks, energy efficiency, multiple-input multiple-output, and cooperative communications.

Ahmed Zoha (M'13) received the Ph.D. degree in electronic engineering, funded by the Engineering and Physical Sciences Research Council, from the University of Surrey, Surrey, U.K., in 2014.

He is currently a Research Scientist with the Qatar Mobility Innovation Center, Doha, Qatar, focusing on self-organizing network solutions, particularly automated fault detection and self-healing aspects of cellular networks. His research interests include machine learning, big data analytics, knowledge discovery, and self-organizing networks.

Jessica Moysen (S'15) received the B.Sc. degree in electronics and communications engineering from the Instituto Tecnológico y de Estudios Superiores de Monterrey Campus Estado de México and the M.Sc. degree in multimedia and communications from the Universidad Carlos III de Madrid, Madrid, Spain, in 2011. She is currently working toward the Ph.D. degree in telecommunication engineering with the Department of Signal Theory and Communication, Universitat Politécnica de Catalunya, Barcelona, Spain, associated with the Centre Tecnòlogic Telecomunicacions Catalunya (CTTC) under a grant from the Spanish Ministry of Science and Innovations.

Her research interests include self-organizing networks, wireless networks, machine learning, and statistical tools to analyze data.

Ali Imran (M'15) received the B.Sc. degree in electrical engineering from the University of Engineering and Technology, Lahore, Pakistan, in 2005 and the M.Sc. degree (with distinction) in mobile and satellite communications and the Ph.D. degree from the University of Surrey, Guildford, U.K., in 2007 and 2011, respectively.

He is an Assistant Professor in telecommunications with the University of Oklahoma, Norman, OK, USA. He is currently leading a multinational $1.045 million research project on self-organizing cellular networks—QSON (www.qson.org). He has authored over 40 peer-reviewed articles. His research interests include self-organizing networks, radio resource management, and big data analytics.

Mr. Imran has presented a number of tutorials at international forums, such as the IEEE International Conference on Communications, the IEEE Wireless Communications and Networking Conference, European Wireless, and the International Conference on Cognitive Radio Oriented Wireless Networks on topics of his interest. He is an Associate Fellow of the Higher Education Academy, U.K., and a Member of Advisory Board to the Special Technical Community on Big Data of the IEEE Computer Society.

Lorenza Giupponi (SM'14) received the degree in telecommunications engineering from the University of Rome La Sapienza, Rome, Italy, in 2002 and the Ph.D. degree from the Department of Signal Theory and Communications, Technical University of Catalonia (UPC), Barcelona, Spain, in 2007.

In 2003, she joined the Radio Communications Group of UPC with a grant from the Spanish Ministry of Education. During 2006–2007, she was an Assistant Professor with the UPC. In September 2007, she joined the CTTC. She is currently a Senior Researcher with the Communication Networks Division, Mobile Networks Department and the Director of Institutional Relations as a member of the CTTC Executive Committee. She has participated in multiple European research projects and has been the Principal Investigator of national and international research projects.

Muhammad Ali Imran (M'03–SM'12) received the M.Sc. (with distinction) and Ph.D. degrees from Imperial College London, London, U.K., in 2002 and 2007, respectively.

He is currently a Reader (Associate Professor) with the Institute for Communication Systems (ICS—formerly known as CCSR), University of Surrey, Surrey, U.K. He has led a number of multi-million international research projects encompassing the areas of energy efficiency, fundamental performance limits, sensor networks, and self-organizing cellular networks. He is currently leading the new physical-layer work area for the fifth-generation innovation center and the curriculum design for the Engineering for Health program at the University of Surrey. He has a global collaborative research network spanning both academia and key industrial players in the field of wireless communications. He has supervised 20 successful Ph.D. graduates and published over 200 peer-reviewed research papers, including more than 20 IEEE TRANSACTION papers.

Mr. Imran has delivered several keynotes, plenary talks, invited lectures, and tutorials at many international conferences and seminars. He has been a Guest Editor for Special Issues in the IEEE COMMUNICATIONS, the IEEE WIRELESS COMMUNICATION MAGAZINE, *IET Communications*, and IEEE ACCESS. He is an Associate Editor of the IEEE COMMUNICATIONS LETTERS and the *IET Communications Journal*. He received the IEEE Communications Society Fred Ellersick Award in 2014 and the Foundation for Eden Prairie Schools Learning and Teaching Award in 2014 and was twice nominated for the Tony Jeans Inspirational Teaching Award. He was a shortlisted finalist for The Wharton-QS Stars Awards 2014 for innovative teaching and the Vice-Chancellor's Learning and Teaching Award at the University of Surrey. He is a Senior Fellow of the Higher Education Academy, U.K.

Adnan Abu-Dayya (SM'14) received the Ph.D. degree in electrical engineering from Queen's University, Kingston, ON, Canada, in 1992.

He has more than 25 years of global experience in the areas of ICT R&D, product innovations, business development, and service delivery. He is currently the Founding Executive Director (CEO) of the Qatar Mobility Innovations Center, Qatar Science and Technology Park, Qatar. He serves on the Advisory Board of the Arab Innovation Network and the Department of Electrical and Computer Engineering, Texas A&M University at Qatar, Doha, Qatar.